RRPB89050593 (5.P)

行政院國家科學委員會專題研究計畫成果報告

燃燒室中燃燒不穩定之火焰轉移函數實驗探討
Experimental investigations of flame transfer function in an acoustically excited combustor

計畫編號：NSC 89-2612-E-032-002
執行期限：88 年 8 月 1 日至 89 年 7 月 31 日

主持人：陳增源 副教授 淡江大學航空太空工程學系
e-mail:yuan@aero.tku.edu.tw

兼任助理：陳建邦、黃漢生

一、中文摘要

本研究實驗探討在聲波激擾管道中，一預混、層流火焰之轉移函數。此轉移函數係由所量測之火焰上、下游聲場強度所決定，其包含火焰上、下游之壓力及速度振盪值。研究結果顯示，火焰轉移函數之正負及大小，與火焰所在之聲波場有絕對關聯；而火焰當量比僅扮演決定轉移函數大小之角色。

Abstract

This research experimentally investigates the flame transfer function in an acoustically excited vertical duct with a laminar, premixed flame anchored on a grid. The flame transfer function is determined from the measured acoustic intensity upstream and downstream of the flame zone, which relates both the acoustic velocities and pressures either side of the flame zone. Results of this research reveal that the location of flame zone on the acoustic field plays the main role in determining the sign and magnitude of the flame transfer function. The flame equivalence ratio plays a role only in the magnitude of the flame transfer function.

二、Introduction

Sound can be generated when a flame is anchored to a grid in a tube. This instability falls in the field of thermoacoustic instability. This acoustic oscillation is closely related to the flame transfer function that describes the response of flames to sound wave disturbances. A good review of these instabilities in Rijke tubes and related devices is provided by Raun et al [1]. Most studies [2-8] of the flame transfer function focused on theoretical investigations. Also, the definitions of flame transfer functions mainly include the acoustic velocities upstream and downstream of the flame zone but not the acoustic pressure that is assumed constant across the flame zone. This research experimentally investigates the flame transfer function in an acoustically excited vertical duct with a premixed flame anchored on a flame holder. The flame transfer function defined in this study includes the pressure distributions upstream and downstream of the flame zone.

三、 Experimental setup and analysis

The configuration of the experimental setup and the three premixed flame burners, which are referred to burners A, B and C, are shown in Fig. 1. It consisted of an 80-*cm* long, 4x8 cm^2 rectangular duct with a premixed flame burner placed into one end of the duct. A 4-*mm* thick ceramic matrix was placed inside the duct 8.5-*cm* above the burner exit plane to act as a flame holder. More detailed description of the experimental system can be referred to Ref. 9. Since the flow velocities used in this research were around 16 *cm/sec*, essentially flat laminar premixed flames were obtained that were stabilized very close to the flame holder.

The flame transfer function defined in this study is based on the acoustic intensity upstream and downstream of the flame zone. The difference in acoustic intensity, ΔI, upstream and downstream of the flame zone can be expressed as:

$$\Delta I = \tfrac{1}{2}|p'|_1^2 \left[\left(|p'|_2^2 / |p'|_1^2\right) Re(Y)_2 - Re(Y)_1\right]$$

where subscripts 1 and 2 denote the conditions upstream and downstream of the flame zone,

$Re(Y)=|u'|/|p'|\cos\phi_{p'u'}$ is the real part of acoustic admittance, and $\phi_{p'u'}$ is the phase difference between the velocity and pressure oscillations. The difference in acoustic intensity upstream and downstream of the flame zone is mainly due to the flame-acoustic wave interaction. The flame transfer function (Tr) is defined as:

$$Tr=[(|p'|_2^2/|p'|_1^2)Re(Y)_2-Re(Y)_1]\rho_1 c_1$$

The flame transfer can be related to the flame driving/damping characteristic. When Tr is positive, acoustic energy is generated in the flame zone and it is said to be driving. On the contrary, when Tr is negative, acoustic energy is absorbed by the flame and it is said to be damping. The flame transfer function is determined from the measured amplitudes of velocity and pressure oscillations, and the phase difference between the velocity and pressure oscillations.

三、Results and discussion

The flame transfer function is closely related to the real parts of acoustic admittances and the pressure amplitudes upstream and downstream of the flame zone. Figures 2 and 3 present the real parts of acoustic admittances upstream and downstream of the flame zones for the three burner systems, which are normalized by the characteristic impedance, $\rho_1 c_1$. It was shown in these figures that the distributions of the real parts of acoustic admittances upstream of the flame zones, $Re(Y)_1$, for hot flow cases exhibit little difference among the test flame equivalence ratios and are similar to those for cold flow cases. This result reveals that the flame has little effect on the acoustic admittance upstream of the flame zone. These figures also show that the distributions of the real parts of acoustic admittances downstream of the flame zone, $Re(Y)_2$, are similar among the test flame equivalence ratios, generally having the largest positive and negative values for the flame equivalence ratio of 1.1. In addition, the $Re(Y)_2$ exhibit sharp changes in magnitude and sign near the frequency of 400 Hz in burner A and B systems, while no sharp change was observed in burner C system. It is also noted that the magnitudes of $Re(Y)_1$ and $Re(Y)_2$ in burner C system are generally smaller than those in burner A and B systems. These results are further discussed by the measured $|u'|/|p'|$ and $\phi_{p'u'}$.

Figure 4 presents the measured amplitude ratios of velocity and pressure oscillations, $|u'|/|p'|$ It was shown in this figure that the $|u'|/|p'|$ are similar among the test conditions. The presence of flame modifies only the values, but not the trend, of $|u'|/|p'|$, and generally results in larger values of $|u'|/|p'|$. These results reveal that the distributions of $|u'|/|p'|$ for hot flow cases are dominated by the distributions of $|u'|/|p'|$ for cold flow cases. The flame equivalence ratio plays a role in determining the magnitude of $|u'|/|p'|$. Figure 4 also shows that there is a sharp increase in the distribution of $|u'|/|p'|$ near the frequency of 375 Hz in burner A system. In addition, this figure shows that the magnitudes of $|u'|/|p'|$ in burner C system are generally smaller than those in burner A system. These results are closely related to the location of flame zone on the acoustic field as presented in Fig. 5, the symbol "d" denotes the distance between the flame location and the nearest pressure node of an acoustic wave inside the duct, and λ is the corresponding wavelength. It is shown in this figure that the flame zones locate at the pressure nodes of the 380 Hz and 420 Hz acoustic waves in burner A and B systems, respectively. Since the flow/flame is mainly subjected to a velocity oscillation at a pressure node, the $|u'|/|p'|$ near the frequency of 375 Hz are the largest among the test frequencies, and exhibit a sharp change near the frequency of 375 Hz in burner A system, as shown in Fig. 4. Similar result was observed in burner B system. On the contrary, the flame zones in burner C system locate closer to the pressure anti-nodes of acoustic waves than those in burner A and B systems for most of the test frequencies. As a result, the values of $|u'|/|p'|$ in burner C system are generally

smaller than those in burner A and B systems, and no sharp change in $|u'|/|p'|$ was observed.

Figure 6 presents the $\phi_{pu'}$ upstream and downstream of flame zones for cold and hot flow cases in burner A and C systems. It was shown in this figure that the distributions of $\phi_{pu'}$ are similar among the cold and hot flow cases, and the values of $\phi_{pu'}$ decrease across the flame zone, depending on the flame equivalence ratio. These results reveal that the distributions of $\phi_{pu'}$ for hot flow cases are dominated by the distribution of $\phi_{pu'}$ for cold flow cases. The flame equivalence ratio is important mainly in determining the amount of phase decrease. It was shown in Fig. 5 that the flame zones locate at the pressure-amplitude decreasing and increasing of acoustic waves for frequencies lower and higher than 380 Hz, respectively, in burner A system. Consequently, the velocity oscillations lag and precede the pressure oscillations for frequencies lower and higher than 380 Hz acoustic wave, respectively, and there is a sharp phase change in the vicinity of 380 Hz, as shown in Fig. 6. On the contrary, since the flame zones in burner C system locate at the pressure-amplitude decreasing of the test acoustic waves, the velocity oscillations lag the pressure oscillations for all of the test frequencies, and no sharp phase change was observed.

Since the distributions of $|u'|/|p'|$ and $\phi_{pu'}$ for hot flow cases are dominated by the respective distributions for cold flow cases, the reactive acoustic admittance is dominated by the nonreactive acoustic admittance. Also, since the $|u'|/|p'|$ and $\phi_{pu'}$ for cold flow cases are closely related to the location of flame zone on the acoustic field, the reactive acoustic admittance is a strong function of the nonreactive acoustic admittance at the flame location. These results show that the acoustic admittance of flame/grid system is dominated by the nonreactive acoustic admittance at the flame location. In addition, since $|u'|/|p'|$ and $\phi_{pu'}$ exhibit sharp changes in their distributions in the vicinity of 375 Hz in burner A system, the *Re(Y)* change sharply from negative to positive near these frequencies, as shown in Fig. 2. No sharp change in *Re(Y)* was observed in burner C system. As discussed above, the velocity oscillations in burner A system precede and lag the pressure oscillations for frequencies higher and lower than 380 Hz, respectively, and the presence of flames results in the decrease of $\phi_{pu'}$. Consequently, the *Re(Y)* downstream of the flame zone have high possibility to be positive for frequencies higher than 380 Hz. On the other hand, the *Re(Y)* downstream of the flame zone would possibly be negative and even less than the *Re(Y)* upstream of the flame zone for frequencies lower than 380 Hz, as shown in Fig. 2. On the contrary, since the velocity oscillations lag the pressure oscillations for all of the test frequencies in burner C system, the *Re(Y)* downstream of the flame zone in burner C system would possibly be negative.

The flame transfer functions were obtained by using the acoustic admittance data and the pressure data. Figures 7 and 8 present the obtained flame transfer functions, *Tr*, of the three investigated burner systems. The flame transfer functions change sharply from positive to negative near the frequency of 375 Hz in burner A system, as shown in Fig. 7. On the contrary, the flame transfer functions in burner C system are small, negative values for all of the test frequencies, and do not exhibit a sharp change in its distribution, as indicated Fig. 8. Since the pressure ratios and the real parts of acoustic admittances upstream and downstream of the flame zone strongly depend upon the nonreactive acoustic admittance at the flame location, the flame transfer function is a strong function of the nonreactive acoustic admittance at the flame location. Figures 7 and 8 also indicate that the distributions of the flame transfer function are similar among the test flame equivalence ratios, indicating that the flame equivalence ratio plays a role mainly in determining the magnitude of the flame transfer function. The sign of the flame transfer function is also determined by the location of flame zone on the acoustic field. The flame transfer function is generally positive and negative when the flame zones locate at the pressure-amplitude

increasing and decreasing of acoustic waves, respectively. In addition, large and small values of the flame transfer functions occur when the flame zone locates near a pressure node and a pressure anti-node of acoustic waves, respectively.

四、Conclusion

Results of this study show that the flame transfer function and the acoustic admittance of the flame/grid system are mainly dominated by the nonreactive acoustic admittance at the flame location. The flame transfer function exhibits sharp changes in magnitude and sign for the flame zone located near a pressure node of acoustic wave. Positive and negative values of the flame transfer functions occur when the flame zone locates at the pressure-amplitude increasing and decreasing of acoustic waves, respectively. In addition, large and small values of the flame transfer functions occur when the flame zones locate close to a pressure node and a pressure anti-node of acoustic waves, respectively. The flame equivalence ratio plays a role mainly in determining the magnitude, not the sign, of the flame transfer function.

五、計畫成果自評

本計畫主要研究內容為探討火焰轉移函數與聲導納、火焰當量比及聲波場頻率之關聯；在本研究中利用聲場強度之量測，包括壓力及速度振盪及其振盪之相位關係，所得結果已達成本計畫之目標，對於燃燒不穩定有進一步之了解。

六、Reference

1. Raun, R. L., Beckstead, J. C., Finlinson, J. C. and Brooks, K. P. (1993). A Review of Rijke Tubes, Rijke Burners and Related Devices, *Prog. Energy Combust. Sci.* 19, 313-364.
2. Mugridge, B. D. (1980). Combustion Driven Oscillations, *Journal of Sound and Vibration* 70(3), 437-452.
3. Nicoli, C. and Pelce, P. (1989). One-dimensional Model for the Rijke Tube, *J. Fluid Mech.* 202, 83-96.
4. McIntosh, A. C. (1986). The Effects of Upstream Acoustic Forcing and Feedback on the Stability and Resonance Behavior of Anchored Flames, *Combustion Science and Technology* 49, 143-167.
5. McIntosh, A. C. (1987). Combustion-Acoustic Interaction of a Flat Flame Burner System Enclosed Within an Open Tube, *Combust. Sci. and Tech.* 54, 217-236.
6. McIntosh, A. C. (1990). On Flame Resonance in Tubes, *Combust. Sci. and Tech* 69, 147-152.
7. McIntosh, A. C. and Rylands, S. (1996). A Model of Heat Transfer in Rijke Tube Burners, *Combust. Sci. and Tech.* 113-114, 273-289.
8. Clavin, P., Pelce, P. and He, L. (1990). One-dimensional Vibratory Instability of Planar Flames Propagating in Tubes, *J. Fluid Mech.* 216, 299-322.
9. Chen, T. Y. and Chen, M. G. (1999). Sound Emission of Ducted Premixed Flames, *Journal of Sound and Vibration* 221(2), 221-234.

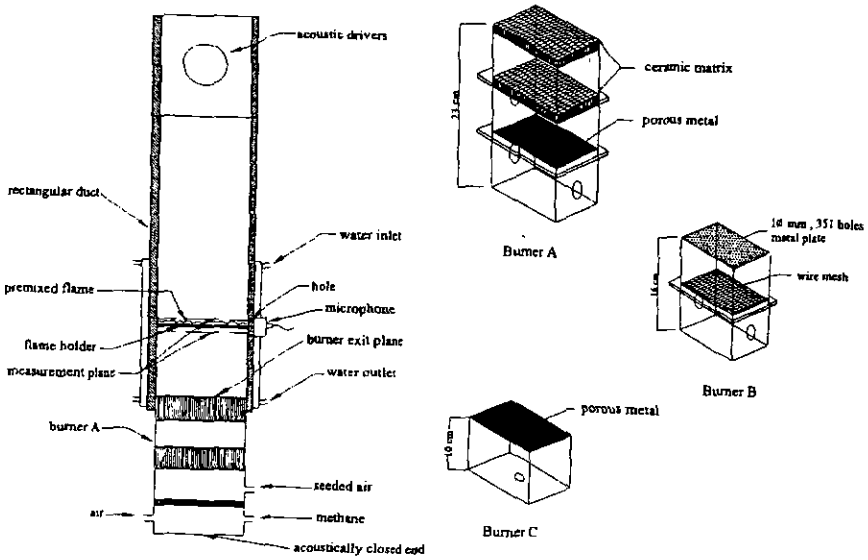

Figure 1: The configuration of the experimental setup and the burner system (not to scale).

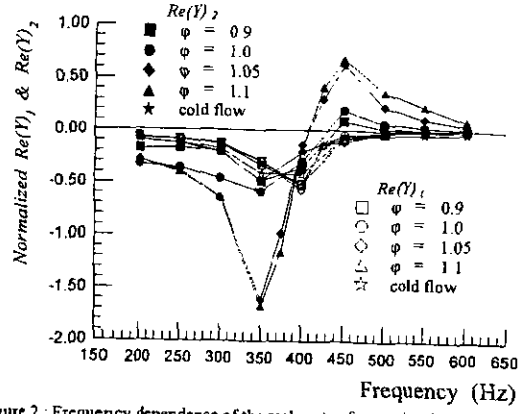

Figure 2 : Frequency dependence of the real parts of acoustic admittances upstream, $Re(Y)_1$, and downstream, $Re(Y)_2$, of the flame zones for cold flow cases and different flame equivalence ratios in burner A system.

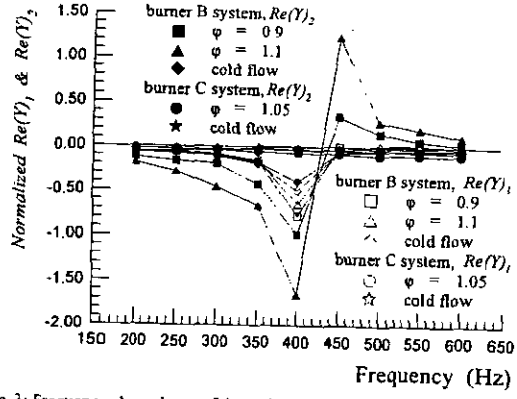

Figure 3: Frequency dependence of the real parts of acoustic admittances upstream, $Re(Y)_1$, and downstream, $Re(Y)_2$, of the flame zones for cold flow cases and different flame equivalence ratios in burner B and C systems

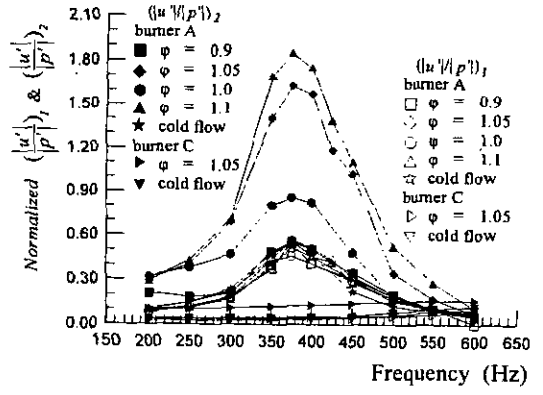

Figure 4 : Frequency dependence of the amplitude ratios of velocity and pressure oscillations upstream, $(|u'|/|p'|)_1$, and downstream, $(|u'|/|p'|)_2$ of the flame zones for cold and hot flow cases in burner A and C systems.

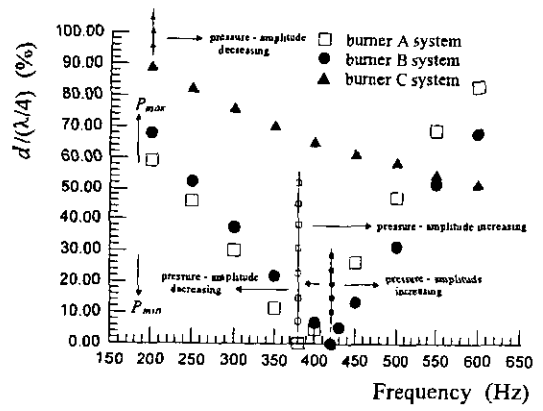

Figure 5 : The locations of flame zones on the acoustic fields for the three test burner systems.

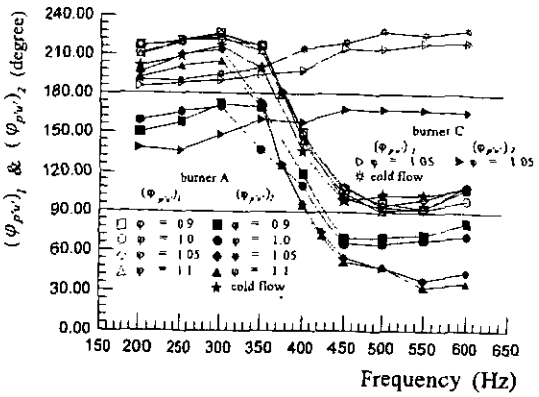

Figure 6: Frequency dependence of the phase differences between the velocity and pressure oscillations upstream, $(\varphi_{p'v'})_1$, and downstream, $(\varphi_{p'v'})_2$, of the flame zone for the cold and hot flow cases in burner A and C systems.

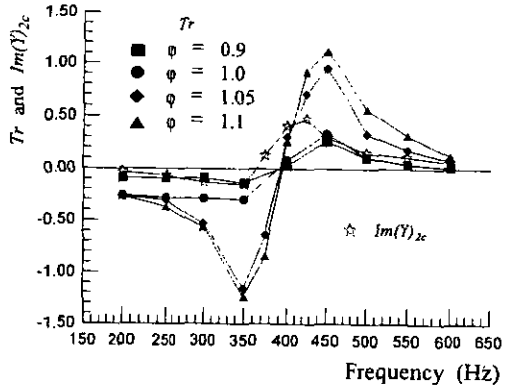

Figure 7 : Distributions of the flame transfer functions, Tr, for different flame equivalence ratios, and the imaginary parts of nonreactive acoustic admittances downstream of the flame zones, $Im(Y)_{2c}$, in burner A system.

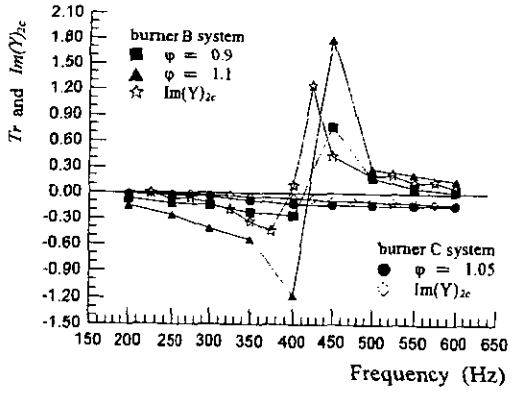

Figure 8: Distributions of the flame transfer functions, Tr, for different flame equivalence ratios, and the imaginary parts of nonreactive acoustic admittances downstream of the flame zones, $Im(Y)_{2c}$, in burner B and C systems.